Energy Engineering

Tech Science Press

Doi:10.32604/ee.2025.073955

ARTICLE

# A Hybrid Artificial Intelligence Model for Accurate Prediction of Gas Emissions in Power Plant Turbines

**Samar Taha Yousif[1,2], Firas Basim Ismail[1,3,*], Ammar Al-Bazi[4], Alaa Abdulhady Jaber[5] and Sivadass Thiruchelvam[1]**

[1]Smart Power Generation Unit, Institute of Power Engineering (IPE), Universiti Tenaga Nasional (UNITEN), Kajang, 43000, Malaysia
[2]College of Engineering, University of Information Technology and Communications, Baghdad, 10066, Iraq
[3]Faculty of Engineering, Sohar University, P.O. Box 44, Sohar, PCI 311, Oman
[4]Operations and Information Management Department, Aston Business School, Birmingham, B4 7ET, UK
[5]Mechanical Engineering Department, University of Technology-Iraq, Baghdad, 10001, Iraq

*Corresponding Author: Firas Basim Ismail. Email: firas@uniten.edu.my

Received: 29 September 2025; Accepted: 21 November 2025; Published: 27 February 2026

**ABSTRACT:** Thermal power plants are the main contributors to greenhouse gas emissions. The prediction of the emission supports the decision makers and environmental sustainability. The objective of this study is to enhance the accuracy of emission prediction models, supporting more effective real-time monitoring and enabling informed operational decisions that align with environmental compliance efforts. This paper presents a data-driven approach for the accurate prediction of gas emissions, specifically nitrogen oxides (NOx) and carbon monoxide (CO), in natural gas power plants using an optimized hybrid machine learning framework. The proposed model integrates a Feedforward Neural Network (FFNN) trained using Particle Swarm Optimization to capture the nonlinear emission dynamics under varying gas turbine operating conditions. To further enhance predictive performance, the K-Nearest Neighbor (K-NN) algorithm serves as a post-processing method to enhance IPSO-FFNN predictions through adjustment and refinement, improving overall prediction accuracy, while Neighbor Component Analysis is used to identify and rank the most influential operational variables. The study makes a significant contribution through the combination of NCA feature selection with PSO global optimization, FFNN nonlinear modelling, and K-NN error correction into one unified system, which delivers precise emission predictions. The model was developed and tested using a real-world dataset collected from gas-fired turbine operations, with validated results demonstrating robust accuracy, achieving Root Mean Square Error values of 0.355 for CO and 0.368 for NOx. When benchmarked against conventional models such as standard FFNN, Support Vector Regression, and Long Short-Term Memory networks, the hybrid model achieved substantial improvements, up to 97.8% in Mean Squared Error, 95% in Mean Absolute Error (MAE), and 85.19% in RMSE for CO; and 97.16% in MSE, 93.4% in MAE, and 83.15% in RMSE for NOx. These results underscore the model's potential for improving emission prediction, thereby supporting enhanced operational efficiency and adherence to environmental standards.

**KEYWORDS:** Natural gas turbines; emission prediction; NOx; CO; FFNN; PSO; K-NN; NCA

## 1 Introduction

The rising concern over declining air quality and environmental degradation has spurred extensive global research efforts. Air pollution stands as one of the most critical environmental threats, with well-established associations to adverse human health outcomes, including respiratory illnesses, cardiovascular conditions, and premature mortality [1]. In urban and industrial zones, the energy sector emerges as a leading contributor to atmospheric pollutants, particularly nitrogen oxides (NOx) and carbon monoxide (CO), emitted predominantly during electricity generation [2].

Natural gas power plants (GPPs), which heavily depend on fossil fuel combustion, are substantial sources of these harmful emissions. While gas turbines within GPPs are vital for delivering high-efficiency electricity, their operation entails complex combustion dynamics that yield variable emissions influenced by factors such as inlet air temperature, combustion pressure, and fuel characteristics. In countries such as Iraq, where power generation facilities often operate near residential areas, these emissions pose serious risks to environmental quality and public health [3]. As a result, enhancing emission prediction accuracy is crucial to support regulatory compliance and operational safety.

The current traditional emission prediction models for gas turbines fail to deliver accurate results when operating under changing conditions because they lack established methods for feature selection, leading to poor performance in real-world applications. This situation highlights an urgent need for intelligent, data-driven systems that can adapt to various operational environments to model complex nonlinear emission patterns.

Numerous studies have explored the use of artificial intelligence (AI) and machine learning (ML) for emission estimation. Predictive Emissions Monitoring Systems (PEMS) emerge as cost-effective alternatives to traditional Continuous Emissions Monitoring Systems (CEMS), which are often expensive and require complex calibration. Among AI tools, Artificial Neural Networks (ANNs) have proven effective due to their ability to model nonlinear combustion dynamics in real-time. For instance, [4] developed ANN-based emission estimators for U.S. power plants, demonstrating their reliability with operational data [5] further enhanced NOx prediction accuracy by combining ANNs with optimization algorithms.

To overcome the limitations of traditional ANN training (e.g., slow convergence and local minima), hybrid models integrating Feedforward Neural Networks (FFNNs) with optimization algorithms such as Particle Swarm Optimization (PSO) have been widely adopted. For example, [6] compared standalone ANN and hybrid PSO-ANN models and found the latter more accurate and robust in emission prediction. Similarly, [7] reported improved convergence and accuracy when applying PSO to NOx emission models. These studies underscore the potential of hybrid ANN-based frameworks to improve emission forecasting in complex operational environments.

The proposed IPSO-FFNN implements a new K-NN guided initialization method, which sets it apart from typical PSO-ANN systems. The IPSO-FFNN system uses K-Nearest Neighbors to predict weight and bias values at startup, which results in faster convergence and better solution quality compared to standard PSO-ANN. The method decreases the chances of particles getting stuck in local minima while using mathematical methods to determine the starting point which makes the training process more reliable.

Despite these advances, emission monitoring in gas turbine systems still presents significant challenges. These include highly variable operating conditions, intricate combustion mechanisms, and the demand for responsive prediction models. Traditional monitoring tools often fail to capture rapid emission changes, particularly in infrastructure-limited regions such as Iraq [8]. Furthermore, emissions from gas turbines can fluctuate by up to 20% due to load variability, adding complexity to prediction models [9]. These challenges highlight the need for intelligent, adaptive systems tailored to real-world conditions.

Conventional regression-based prediction methods have generally underperformed in such settings. They struggle to generalize across changing loads and ambient conditions like high temperatures and humidity [10]. Moreover, many fail to include feature selection or advanced optimization, reducing their applicability in operational environments.

To address these gaps, this study presents a robust data-driven hybrid machine learning framework that integrates a PSO-optimized FFNN with K-NN for refining predictions and NCA for feature selection, thereby enhancing the accuracy and adaptability of NOx and CO emission predictions under varying turbine operating conditions. The proposed hybrid framework achieves its goals through the combination of its individual components. The NCA method selects essential turbine parameters that decrease input size and remove unnecessary features that could harm model accuracy. The PSO algorithm performs global weight optimization for FFNN to solve the common problems of slow training and getting stuck in local minima points. The K-NN algorithm performs residual smoothing by predicting errors from neighboring points to enhance output precision and prevent overfitting when operating under changing conditions. The system achieves adaptive learning and fast convergence, as well as improved robustness for emission prediction, through its combined elements. This combination enables the model to adaptively focus on the variables that most significantly influence emissions under real-world operating conditions.

The model received its training data from the Al-Quds power plant, but its ability to predict turbine behavior under different specifications, fuel types, and climate conditions remains untested.

This hybrid methodology offers a practical, scalable solution that improves predictive accuracy and supports better real-time emission management. The model contributes to the field by addressing a key research gap: the need for robust, adaptive, and interpretable prediction tools capable of operating effectively under dynamic and resource-constrained conditions.

## 2 Neural Networks in Predictive Emission Monitoring

Neural networks (NNs) have garnered significant interest in predictive emission monitoring for gas turbines due to their ability to learn complex, nonlinear relationships from operational data [11] highlighted that both deep and feedforward architectures of neural networks effectively model dynamic emission behaviors across varying operational conditions. Among these, Feedforward Neural Networks (FFNNs), a subset of Artificial Neural Networks (ANNs), are particularly popular due to their adaptability and generalization capabilities [12] illustrated this flexibility in a maritime context by developing an ANN model that predicted NOx and CO emissions based on engine load and shaft speed. The model achieved an $R^2$ value of 0.977, emphasizing the reliability of neural networks in fluctuating environments. Building on such promising results, researchers have increasingly explored hybridizing ANN models with optimization algorithms to further improve predictive performance. Ref. [6] conducted a comparative study, showing that hybrid models integrating metaheuristic techniques like Particle Swarm Optimization (PSO) and Genetic Algorithms (GA) consistently outperformed standalone ANN models. These hybrids demonstrated improved convergence rates and reduced generalization errors. Similarly, Ref. [13] validated the superiority of FFNNs over traditional regression methods in predicting $NO_x$ emissions, with lower mean absolute errors observed.

However, several limitations persist. Many models fail to accommodate real-time operational variability, resulting in potential overfitting and diminished generalization performance. Additionally, hybrid models such as PSO-ANN and GA-ANN, while accurate, are computationally demanding and sensitive to parameter tuning factors that constrain scalability and real-time applicability. These challenges underscore the need for more efficient, adaptive approaches to neural network optimization in emission monitoring.

### 2.1 Particle Swarm Optimization for Neural Networks

Particle Swarm Optimization (PSO), introduced by Kennedy and Eberhart in 1995, is a nature-inspired algorithm that mimics the social behavior of bird flocks and fish schools. Each particle represents a candidate solution (e.g., a set of neural network weights) and iteratively updates its position by considering both its best-known position and the swarm's global best. This process enables efficient exploration of high-dimensional search spaces, making PSO well-suited for neural network training.

Tuttle [7] demonstrated that PSO significantly accelerates convergence during neural network training for $NO_x$ emissions prediction, surpassing traditional gradient-based approaches. Ref. [14] applied PSO to deep learning architectures for $CO_2$ emission prediction and achieved reductions in overfitting. Similarly, Ref. [15] developed a multi-objective PSO framework that successfully balanced prediction accuracy with computational efficiency in emission control tasks.

Recent innovations further demonstrate PSO's versatility. Ref. [16] enhanced a backpropagation NN for shale gas prediction using PSO and grey relational analysis for feature selection, achieving superior accuracy compared to conventional methods. Ref. [17] proposed a PSO-based method for structuring reservoir computing models, which showed promising results in time-series prediction.

Despite these strengths, standard PSO faces limitations, including premature convergence and susceptibility to local minima. Additionally, computational demands remain a concern for real-time and large-scale applications. These drawbacks have spurred further research into enhanced and hybridized PSO variants.

### 2.2 Advances in Swarm Intelligence for Neural Network Optimization

To overcome the limitations of standard PSO, hybrid and alternative swarm intelligence algorithms have been explored, offering enhanced exploration and convergence capabilities.

Hybrid PSO models combine PSO with other optimization or learning strategies to improve performance. For instance, Ref. [18] developed a DPSO-PSO-FFNN framework by integrating discrete and standard PSO with the Levenberg-Marquardt algorithm. This hybrid approach significantly improved training efficiency and predictive accuracy. Ref. [19] introduced PSOCoG, which integrates a center-of-gravity mechanism to better balance global and local search phases. Ref. [20] utilized a modified PSO with time-varying acceleration coefficients to adaptively shift from exploration to exploitation. Similarly, Ref. [21] proposed a hybrid PSO model incorporating cellular automata (HPSO-CA), which mitigated premature convergence and preserved swarm diversity during emission prediction tasks.

Beyond PSO, various swarm-based techniques have been explored for emission prediction. Algorithms like Ant Colony Optimization (ACO), Artificial Bee Colony (ABC), and Firefly algorithms provide different mechanisms for navigating complex search spaces. Ref. [22] demonstrated that applying these algorithms to neural network training led to improved prediction accuracy in emission tasks.

The Dragonfly Algorithm (DA), which models dragonfly swarming behavior, has been hybridized with ABC to create HAD (Hybrid ABC-DA). Ref. [23] showed this hybrid provided improved balance between exploration and exploitation. Ref. [24] proposed the Harris Hawks Optimization (HHO) algorithm, inspired by hawk hunting strategies, which performed well in large-scale optimization contexts.

### 2.3 Comparative Performance Analysis

A comparative analysis of swarm intelligence algorithms highlights their diverse performance in training neural networks. As shown in Table 1, standard PSO remains the most widely used algorithm due to its simplicity and proven performance. However, hybrid PSO variants have demonstrated superior results, especially in tasks involving complex and non-convex search spaces.

**Table 1:** Training feedforward neural networks using the particle swarm optimization algorithm

| Cite | Proposed model | Computational cost | Performance | Applicability |
|---|---|---|---|---|
| [18] | Discrete particle swarm optimization (DPSO) | Iteration = 100 | MAE = 2.53E−04–6.00E−03 RMSE= 1.59E−02–7.78E−02 MAPE = 7.57 | Suitable for optimizing ANNs in complex, nonlinear problems |
| [19] | Enhanced PSO algorithm with the center of gravity (PSOCoG) | Iteration = 100 | MAE = 0.224702–1.19491E−05 MAPE =0.0023%–0.001719% | Applicable for time-series prediction tasks |
| [20] | Modified PSO (MPSO) | Iteration = 200 | MAE = 0.0435–0.0116 RMSE= 0.0616–0.0164 $R^2$ = 0.9248–0.9885 | Suited for optimization tasks requiring both global and local optimization methods |
| [21] | Hybrid PSO and Cellular Automata (CA) strategy | Iteration = 30 | MSE= 0.0096–0.2002 MAE= 0.0574–0.3249 | Suitable for optimization problems in neural networks |
| [25] | Standard PSO algorithm | Iteration = 500 | AUC =0.89, F-Measure = 0.66 | Applicable for structure learning in Bayesian networks |
| [26] | Standard PSO algorithm | Iteration = 200 | MSE = 0.005 | Suitable for time-series forecasting and economic prediction tasks |
| [27] | Hybrid PSO and gene expression programming (PSO-GEP) | Iteration = 150 | RMSE = 2.67 $R^2$ = 0.87 | Effective for controlling multi-agent systems and optimizing formation tasks in dynamic environments |
| [28] | Hybrid PSO and BA with Acceleration Coefficients (MHPSO-BAAC) | Iteration = 1000 Time (s) = 105.1361 | MAPE = 1.12% MAE = 0.0112 RMSE = 0.0577 | Effective for solving eco-friendly and economic dispatch problems |

(Continued)

**Table 1 (continued)**

| Cite | Proposed model | Computational cost | Performance | Applicability |
|---|---|---|---|---|
| [29] | Standard PSO algorithm | — | RMSE = 0.515–1.264 | Applicable for optimizing software testing processes |
| [30] | Combining PSO, neighbor search, and Mantegna-Lévy flight (LPSONS) | Time = 226.888 | MSE = 0.0299<br>Accuracy = 97.56%<br>F-measure =0.6532 | Suitable for complex classification tasks |
| [31] | Standard PSO algorithm | Iteration = 50 | Accuracy = 98.0% | Suitable for developing efficient intrusion detection systems |
| [32] | Standard PSO algorithm | Iteration = 1000 | RMSE = 68.87<br>NSE = 0.90<br>$R^2$ = 0.9 | Applicable for modeling complex rainfall-runoff relationships |
| [33] | PSO-enhanced deep model for crop yield prediction | Iteration = 600 | RMSE = 0.057 | Agriculture yield forecasting |
| [34] | Hybrid deep learning and PSO for predictive maintenance | Iteration = 1000 | RMSE = 0.021<br>$R^2$ = 0.987 | Power plants maintenance |
| [35] | Federated PSO for smart grid energy management | Iteration = 500 | Accuracy = 96.7% | Smart grid applications |

Furthermore, performance metrics such as Mean Squared Error (MSE), Mean Absolute Error (MAE), Root Mean Squared Error (RMSE), Mean Absolute Percentage Error (MAPE), and R-squared ($R^2$) are commonly used to assess the performance of an optimized neural network.

### *2.4 Benchmarking Studies on Gas Power Plant Emissions*

Benchmarking is an essential process for evaluating and improving the performance of predictive models in gas power plants. The use of real-world datasets, as seen in studies [36–39], is crucial for ensuring that the models are both accurate and generalizable. Table 2 provides a summary of various benchmarking

studies focused on gas power plant emissions, demonstrating the diverse methodologies and contributions made by different researchers.

**Table 2:** Summary of benchmarking studies on gas power plant emissions

| Authors | Field of study gas power plant emissions | Collecting real dataset | Data preparation framework | NN for predication | Hybrid NN for predication | Hybrid (NN + IPSO) for predication | 1HL | More than 1HL | Input optimization | NN topology optimization | Performance Indicator MSE, MAE, RMSE, MAPE, and $R^2$ | Specialized code |
|---|---|---|---|---|---|---|---|---|---|---|---|---|
| [26] | √ | √ | √ | | √ | | √ | | √ | √ | √ | |
| [27] | √ | √ | √ | √ | | | | √ | √ | √ | | |
| [28] | | √ | | | | | √ | √ | √ | | √ | |
| [40] | √ | √ | | | √ | | | √ | √ | | √ | |
| [41] | √ | | √ | √ | | | √ | | | √ | | |
| [42] | √ | | | | √ | | | √ | | | √ | |
| [43] | | | | √ | | | | √ | | | | |
| [44] | √ | | | √ | | | | √ | √ | | √ | √ |
| Current study | √ | √ | √ | | | √ | √ | | √ | √ | √ | √ |

A key observation from these studies is the increasing use of hybrid neural networks, which combine standard NNs with optimization algorithms to improve predictive performance by achieving better performance indicators such as reduced MSE, MAE, RMSE, MAPE, and $R^2$.

## 3 Comparative Analysis of Emission Prediction Models

To better illustrate the advantages of the proposed IPSO-FFNN model, Table 3 summarizes the key differences between existing emission prediction techniques and our approach.

**Table 3:** Performance comparison of emission prediction models

| Model | Strengths | Limitations |
|---|---|---|
| Traditional ANN | Easy implementation, adaptive learning | Prone to local minima, slower convergence |
| SVR regression method | Improved accuracy and efficiency | No standard kernel function selection |
| RNN/LSTM | Handles sequential data, captures dependencies | Requires large datasets, high training cost |
| GA-Optimized FFNN | Strong exploration capabilities | Risk of overfitting, slow convergence |
| Standard PSO-FFNN | Faster convergence, fewer hyperparameters | Prone to premature convergence, limited exploration |

(Continued)

**Table 3 (continued)**

| Model | Strengths | Limitations |
|---|---|---|
| Proposed IPSO-FFNN | Improved accuracy, balance of exploration/exploitation | Addresses overfitting, faster convergence, and minimum computational cost |

To address these limitations, the IPSO-FFNN model introduces an enhanced optimization mechanism, combining PSO's exploration strengths with adaptive learning, achieving higher accuracy in NOx and CO emission predictions.

## 4 Methodology

The subsequent subsections provide an in-depth exploration of the techniques utilized, beginning with the Levenberg–Marquardt training algorithm, which is pivotal in optimizing the performance of the FFNN. In this study, the network architecture consists of a single hidden layer, with 30 neurons, and the sigmoid activation function used to map inputs to outputs. The structure is designed to minimize computational complexity while achieving accurate gas emission predictions. Additionally, a diagram of the network architecture is provided in Fig. 1, which illustrates the arrangement of input, hidden, and output layers.

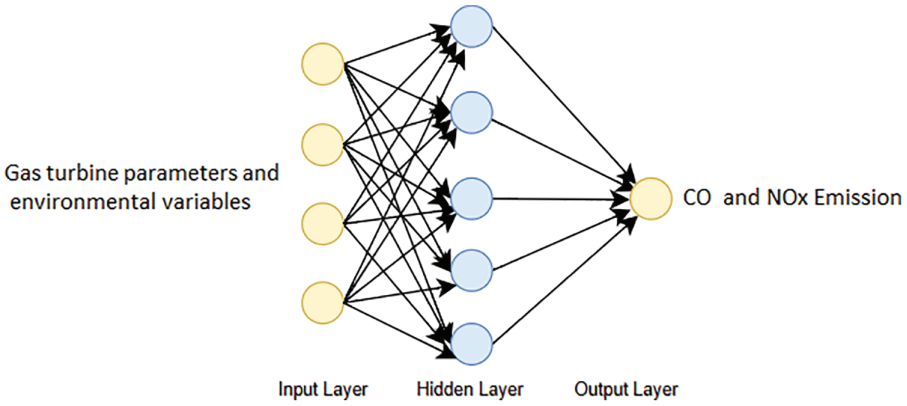


**Figure 1:** The FFNN structure diagram

### *4.1 Levenberg–Marquardt Training Algorithm*

The Levenberg–Marquardt (LM) algorithm is a robust optimization technique employed to fine-tune the weights and biases of FFNNs by minimizing the loss function. This process enhances the model's predictive accuracy and offers several distinctive benefits over traditional optimization methods, making it particularly favorable in the field of computer vision.

### *4.2 Activation Functions*

This study focuses exclusively on the sigmoid activation function, denoted by $\sigma(x)$, defined by the Eq. (1):

$$\sigma(x) = \frac{1}{(1 + e^{-x})} \tag{1}$$

The sigmoid function is chosen for its output range, which is limited to (0, 1). This range aligns seamlessly with the values obtained through min-max normalization, which spans from 0 to 1. Therefore, the use of the sigmoid function is deemed appropriate due to its capacity to produce outputs within the desired range, facilitating compatibility with the normalization process.

### *4.3 Number of Hidden Layers and Neurons*

Previous studies in gas emission prediction often utilize two or three hidden layers. However, adding more layers can significantly increase computational costs and processing times due to additional delays during both training and testing. To optimize efficiency, this study focused on a single hidden-layer FFNN. Preliminary experiments were conducted with varying neuron counts, and a configuration of thirty neurons was selected. This setup balanced model complexity with computational efficiency, achieving optimal performance with minimal overfitting for the dataset.

### *4.4 Dataset Division*

Dataset division is a crucial step in model training, with several common proportions used for splitting data into training, validation, and testing sets. Table 4 summarizes typical ratios reported by [45].

**Table 4:** Common dataset division ratios for training, validation, and testing

| Training (%) | Validation (%) | Testing (%) |
|---|---|---|
| 50 | 40 | 10 |
| 60 | 20 | 20 |
| 70 | 15 | 5 |
| 80 | 10 | 10 |
| 90 | 5 | 5 |

Selecting appropriate proportions is often guided by existing literature and past experiences. Thus, the ratios for dividing the training, validation, and testing sets were optimized based on predicted metrics, including MSE, RMSE, and MAE.

The dataset used for this study was collected from a real-world natural gas power plant. The data span a period of five years (2015–2019), with a total sample size of 39,672 records, and include gas emission measurements (CO and $NO_x$), along with operational parameters such as turbine temperature and pressure. The data was recorded at hourly intervals using sensors. A statistical summary of the dataset is provided in Table 5.

**Table 5:** Statistical summary of key dataset features

| Year | Number of hours | Mean value | Standard deviation |
|---|---|---|---|
| 2015 | 7933 | 280.358 | 375.936 |
| 2016 | 7945 | 280.322 | 375.720 |
| 2017 | 7906 | 281.011 | 374.584 |
| 2018 | 7968 | 280.537 | 374.270 |
| 2019 | 7920 | 280.647 | 374.102 |

Before being fed into the neural network models, the dataset underwent several preprocessing steps, including:

- Data Cleaning: The analysis used linear interpolation to replace missing data, which accounted for 2.3% of all records and removed outliers through statistical z-score thresholds at $|z| > 3$.
- Normalization: Min-max scaling was applied to standardize the range of features to [0, 1], ensuring uniform contribution to the model.
- Feature Selection using NCA: Neighborhood Component Analysis was employed for feature selection to optimize the feature space and improve classification accuracy. NCA learns a distance metric that assigns weights to features based on their importance. This technique effectively retains critical information while reducing noise in the dataset.

The NCA identified Compressor Discharge Pressure, Turbine Inlet Differential Pressure, Compressor Inlet Pressure, Ambient Air Temperature, and Turbine Exhaust Temperature as the top operational variables that affect CO and NOx emissions.

The selection of the optimal training/validation/test ratio for each model was empirically validated. For the standard FFNN model, the best results (lowest MSE, RMSE, and MAE) were obtained with a 50%, 40%, and 10% split. For the Improved PSO-FFNN model, a 60%, 20%, and 20% split yielded optimal performance. These outcomes are consistent with prior benchmarking work [25].

The dataset comprises real field data collected from an operational natural gas power facility located in Iraq. Emission metrics, including CO and NOx concentrations, were obtained through Continuous Emission Monitoring Systems (CEMS), while operating parameters such as turbine inlet temperature, pressure, electrical load, and ambient humidity were recorded using SCADA-based industrial sensors. Data collection was conducted over a five-year period, with each record verified by plant engineers to ensure reliability. This real-time dataset reflects the true operating conditions of Iraqi power generation units and serves as a foundation for robust machine learning model training and validation.

### *4.5 Freezing the Feedforward Neural Network Model*

Weights were fixed after 22 epochs based on empirical convergence patterns to stabilize model output. This eliminated further training and ensured reproducibility.

### *4.6 Improved Particle Swarm Optimization-Feedforward Neural Network Model*

To enhance the model's performance, new configurations (refer to Table 6) were applied, and the PSO algorithm was utilized to optimize the weight coefficients, accelerating convergence and improving the model's learning efficiency. The optimized weights are subsequently integrated into the FFNN model, where the weights are updated in each training cycle to minimize the cost function. This iterative process continues until the global optimum is reached, ensuring the highest possible prediction accuracy.

**Table 6:** Configurations of the IPSO-FFNN model

| Parameter | Value |
|---|---|
| Number of hidden layers | Single (1) |
| Target training performance (MSE) | $1 \times e^{-201}$ |
| Training model | Levenberg–Marquardt algorithm (LM) |
| Minimum gradient | $1 \times e^{-101}$ |

(Continued)

**Table 6 (continued)**

| Parameter | Value |
|---|---|
| Maximum failures | 100 |
| Epoch | 22 |
| Training time goal (seconds) | 30 |
| PSO search space upper bound | +1.09 |
| PSO search space lower bound | −1.09 |

The PSO algorithm optimizes the weight coefficients by adjusting the particle velocity and position to minimize the MSE of the predicted emissions. The velocity of the i-th particle at time t is updated according to Eq. (2):

$$\mathrm{v}_i(t+1) = W \times v_i(t) + c_1 \times R1 \times \left(p_i^{best} - x_i\left(t\right)\right) + c_2 \times R2 \times \mathrm{g}_{best} - x_i\left(t\right)\right) \tag{2}$$

where:

- $\mathrm{v}_i(t+1)$ is velocity of particle $i$ at time $t+1$
- $W$ is inertia weight
- $c_1, c_2$ are acceleration constants
- $R1, R2$ are random values between [0, 1]
- $x_i\left(t\right)$ is the current position (weight) of particle $i$
- $p_i^{best}$ represents the personal best position of particle $i$
- $\mathrm{g}_{best}$ represents global best position

The position of each particle is then updated as in Eq. (3):

$$\mathrm{x}_i\left(t+1\right) = x_i\left(t\right) + \mathrm{v}_i(t+1) \tag{3}$$

The fitness function used to evaluate the solution quality is the MSE of the predictions, given by Eq.(4):

$$MSE = \frac{1}{N}\sum_{i=1}^{N}(T_i - \hat{T_i})^2 \tag{4}$$

where:

- $T_i$ represents true emission values
- $\hat{T_i}$ represents predicted values from the FFNN model
- $N$ represents the total number of test samples

PSO begins by generating a set of weights (particles) and searches for weights that minimize the fitness function by adjusting parameters like inertia weight and velocity [46]. The PSO parameters, such as swarm size, inertia weight, and acceleration constants, were optimized based on preliminary tuning experiments to ensure faster convergence and improved accuracy. These parameters are adjusted to strike a balance between exploration (searching across the solution space) and exploitation (refining the search around the best solutions), leading to a more efficient search for optimal weights.

An innovative IPSO-FFNN algorithm is provided in Algorithm 1, addressing the interaction between PSO optimization, FFNN training, and performance evaluation phases. This algorithm aids in understanding how improved PSO enhances FFNN by iteratively optimizing weight configurations. The PSO optimization

process ensures that the FFNN's performance is maximized by fine-tuning the weights at each training cycle, ultimately resulting in more accurate emission predictions.

**Algorithm 1:** Innovative IPSO-FFNN algorithm.

// ------STAGE 1: Swarm Initialisation --------
Step 1.1: Set Initial Parameters
numParticles ← N
maxIterations ← T
w ← Inertia_Weight
c1, c2 ← Acceleration_Coefficients
Step 1.2: Initialise Particle Population
For each particle i ∈ [1, N]:
$x_i$ ← KNN$_i$nitialise(TrainingData) // initial weights
$v_i$ ← Random$_i$nitial_Velocity
$p_i$ ← $x_i$
Evaluate Fitness: Fitness[i] ← MSE($x_i$, TrainingData)
Step 1.3: Initialise Global Best
g ← argmin(Fitness[i])
// -------- STAGE 2: PSO Optimisation Loop --------
Repeat while iteration < maxIterations:
Step 2.1: Update Particle Velocities
For each particle i ∈ [1, N]:
r1, r2 ← Random(0, 1)
$v_i$ ← w * $v_i$ + c1 * r1 * ($p_i$ − $x_i$) + c2 * r2 * (g − $x_i$)
Step 2.2: Update Particle Positions
$x_i$ ← $x_i$ + $v_i$
Step 2.3: Re-evaluate Fitness
Fitness[i] ← MSE($x_i$, TrainingData)
Step 2.4: Update Personal and Global Bests
If Fitness[i] < MSE($p_i$):
$p_i$ ← $x_i$
If MSE($p_i$) < MSE(g):
g ← $p_i$
// -------- STAGE 3: FFNN Model Construction --------
Step 3.1: Configure FFNN Architecture
FFNN ← CreateNetwork(InputSize, HiddenLayers, OutputSize)
Step 3.2: Inject Optimised Weights
FFNN.Weights ← g
Step 3.3: Train FFNN Using Training Data
Train FFNN on TrainingData using injected weights
// -------- STAGE 4: Output Results --------
Output:
- Final FFNN model
- Optimal weight vector g
- Final MSE score
- Optional training metrics (loss curve, accuracy, etc.)

The above algorithm presents a framework for the training of feedforward neural networks (FFNNs) through the application of Particle Swarm Optimization (PSO). The procedure commences with the definition of swarm parameters, followed by the initialization of a population of particles, each representing a candidate solution comprising a vector of FFNN weights. The KNN algorithm is used for particle position initialization, where it places particles near areas likely to lead to optimal solutions in the search space. The method begins the search with weights that reflect successful local patterns in the data, resulting in quicker search efficiency. The fitness of each particle is evaluated using the mean squared error (MSE) between the network's predicted outputs and the actual target values. During each iteration, particle velocities and positions are updated using the standard PSO update rules, which incorporate both personal and global best positions. The global best solution obtained at the end of the iterative process is then embedded into the FFNN structure, serving as the initial weight configuration. The network is subsequently trained on the dataset, benefiting from the PSO-derived optimization. This hybrid approach leverages the global search capabilities of PSO and the learning power of neural networks, while the KNN-informed initialization promotes improved exploration efficiency and solution quality.

### *4.7 Improved Particle Swarm Optimization-Feedforward Neural Network Model*

The seed generation process in the IPSO-FFNN model involves initializing weights to accelerate convergence. A random seed is generated, denoted as SeedRG Eq. (5), based on the optimum weights from the standard FFNN and adjusted by random values. This approach provides a foundation for optimizing particle positions in the swarm, leveraging well-performing weight configurations as starting points.

$$SeedRG = [length(optimum\ weight), [optimum\ weight\ of\ FFNN] + PRG(R1, R2, [1,1])] \tag{5}$$

### *4.8 Specifications of IPSO Parameters*

The IPSO algorithm's parameters are carefully selected to control the swarm's behavior and convergence rate. The selection of these parameters combined literature recommendations with preliminary experiments and sensitivity analysis to achieve optimal convergence and solution quality. Key parameters are illustrated in Table 7:

**Table 7:** Specifications of IPSO parameters

| Parameter | Value | Range | Selection rationale |
|---|---|---|---|
| Swarm size (S) | 100 | [10–1000+] | The selection process aimed to achieve both exploration and computational efficiency through testing different values of 50, 100, and 200 until 100 produced the optimal results |
| Acceleration constants (c1) | 2 | [0–4] | Adjusted through testing to achieve proper particle movement toward their best positions |
| Acceleration constants (c2) | 2 | [0–4] | Adjusted through direct particles toward the global best solution without exceeding it |
| Inertia weight (W) | 1 | [0–1] | Starting with 1 as its initial value, before using a damping factor to achieve stable swarm movement |

(Continued)

**Table 7 (continued)**

| Parameter | Value | Range | Selection rationale |
|---|---|---|---|
| Number of iterations | 100 | [100–1000+] | The number of iterations was selected through empirical testing, where additional iterations beyond 100 did not produce significant improvements in error measurement results |
| Damping factor | 0.5 | [0.1–0.9] | Controlling the speed of inertia decreases to achieve better stability during convergence |

### *4.9 RNN/LSTM Model*

The RNN/LSTM model in this study is designed for nonlinear prediction, tailored to capture time-based patterns in gas emission data where traditional linear models are inadequate. This LSTM setup includes two hidden layers, chosen after evaluating various configurations for optimal accuracy and processing time. Preprocessing steps involve normalizing inputs and applying Principal Component Analysis (PCA) to reduce features to nine dimensions, making the data manageable while retaining critical information. Model training employs the Adam optimizer with an MSE loss function over 30 epochs. The trained model is then assessed for accuracy, MSE, MAE, RMSE, MAPE, and $R^{2,}$ confirming its capability to handle time dependencies for accurate emission prediction.

## 5 Model Validation

The IPSO-FFNN model validation process involved a thorough evaluation using an independent validation dataset, which was set apart during the first dataset partitioning stage. The model's ability to generalize was evaluated through standard statistical metrics, including (i.e., MSE, RMSE, MAE, MAPE, and $R^2$), which were applied to both CO and NOx emission predictions. The model's performance was validated through output comparison with standard FFNN and RNN/LSTM models before moving on to SVR and K-NN models in an expanded analysis using the same emission dataset.

## 6 Model Comparison

Once the proposed solution is sufficiently developed, it undergoes a comparative evaluation against two baseline models: the standard FFNN and the RNN/LSTM. The standard FFNN provides a foundational benchmark for accuracy and efficiency, while the RNN/LSTM model offers insights into the effectiveness of recurrent architectures for emission prediction. The performance metrics for standard FFNN in predicting CO and $NO_x$ emissions are derived from Eq. (6):

$$E = T - TR \tag{6}$$

where $T$ represents true labels and TR denotes predicted labels. Non-zero values in the error vector indicate errors in predictions, while zero values signify correct predictions. Eq. (7) calculates *MSE*, *MAE*, and *RMSE*:

$$MSE = \sum_{n=1}^{K} \frac{E[K]^2}{K} \tag{7}$$

$$MAE = \sum_{n=1}^{K} \frac{|E[K]|}{K}$$

$$RMSE = \sqrt{\frac{\sum_{n=1}^{i} e(n)^2}{i}}$$

## 7 Results and Discussion

This section presents the findings from applying the IPSO-FFNN model for predicting CO and NOx emissions in a natural gas power plant. The model's performance was analyzed, and its improvement due to PSO optimization was thoroughly discussed. The error analysis is followed by a comparative evaluation with other machine learning models. The results are presented through tables and figures.

### *7.1 Model Performance*

The IPSO-FFNN model demonstrated a significant improvement in predicting CO and NOx emissions compared to the standard FFNN. The model was assessed based on several metrics, as mentioned earlier. Table 8 summarizes the performance metrics results for CO and NOx predictions.

**Table 8:** Performance of IPSO-FFNN vs. standard FFNN in CO and $NO_x$ prediction

| Model | Emission type | MSE | MAE | RMSE | MAPE (%) | $R^2$ |
|---|---|---|---|---|---|---|
| FFNN | CO | 5.756 | 2.182 | 2.399 | 18.252 | 0.704 |
| | NOx | 4.779 | 2.061 | 2.186 | 19.834 | 0.747 |
| IPSO-FFNN | CO | 0.126 | 0.109 | 0.355 | 5.203 | 0.104 |
| | NOx | 0.135 | 0.134 | 0.368 | 4.788 | 0.161 |
| RNN/LSTM | CO | 0.434 | 0.659 | 0.537 | 17.832 | 0.852 |
| | NOx | 0.838 | 0.757 | 0.915 | 29.537 | 0.557 |

The IPSO-FFNN achieved an MSE of 0.126 for CO emissions and 0.135 for NOx, demonstrating superior accuracy in predicting emission levels. The significant reduction in RMSE, from 2.399 to 0.355 for CO and from 2.186 to 0.368 for NOx, underscores the model's improved precision over the standard FFNN. It should be noted that the model depends on both the quantity and precision of sensor data, which serves as input features for its operation. The IPSO-FFNN model will experience decreased predictive accuracy when sensors experience drift or failure or when only a few measurement parameters are available. The reliability of emission predictions depends on maintaining continuous high-quality sensor measurements.

RMSE, as a metric that penalizes larger errors more heavily, highlights the IPSO-FFNN's ability to minimize variance in predictions effectively. Furthermore, compared to benchmarks in the literature, these RMSE values are notably lower than those achieved by traditional models, as reported in studies like [41,42,47,48], where RMSE values for CO and NOx emissions typically ranged from 0.284 to 8.921. This comparison highlights the efficiency of the IPSO-FFNN model in emission prediction tasks. As Algorithm 1 illustrates, the predicted values closely align with the actual emission data across the test set, further validating the model's precision and reliability. In contrast, the RNN/LSTM model, while performing well, achieved higher MSE and RMSE values of 0.434 and 0.537 for CO, and 0.838 and 0.915 for NOx, respectively. These results indicate that the LSTM model struggled with capturing the finer patterns in the emission data when compared to IPSO-FFNN. The LSTM model, being more complex, is often better suited for capturing temporal dependencies in sequential data, but the emission dataset used in this study was recorded at hourly

intervals, resulting in weak long-term temporal connections at this measurement scale, leading to relatively higher prediction errors. Nevertheless, the LSTM model's results still demonstrate a significant improvement over traditional FFNN models, as reflected in the lower RMSE and MSE values for both CO and NOx emissions compared to standard FFNN results.

Moreover, the five-year dataset used in this study adds significant practical value to these results. The model demonstrates operational stability through its ability to handle real-world operational noise and load fluctuations, and ambient condition variations that occur in demanding industrial settings. The model demonstrates superior generalization ability because it operates with actual power plant data instead of simulated information.

In Fig. 2, the alignment between the actual and predicted CO and NOx emissions demonstrates the accuracy of the IPSO-FFNN model. The solid blue lines represent the actual emissions, while the red dashed lines indicate the model's predictions. The model captures the periodic fluctuations of both CO and NOx emissions, reflecting its effectiveness in learning the underlying patterns in the data. The minimal difference between the actual and predicted curves demonstrates the model's high accuracy in capturing emission variations, supported by the low MSE, MAE, and RMSE values detailed in Table 5.

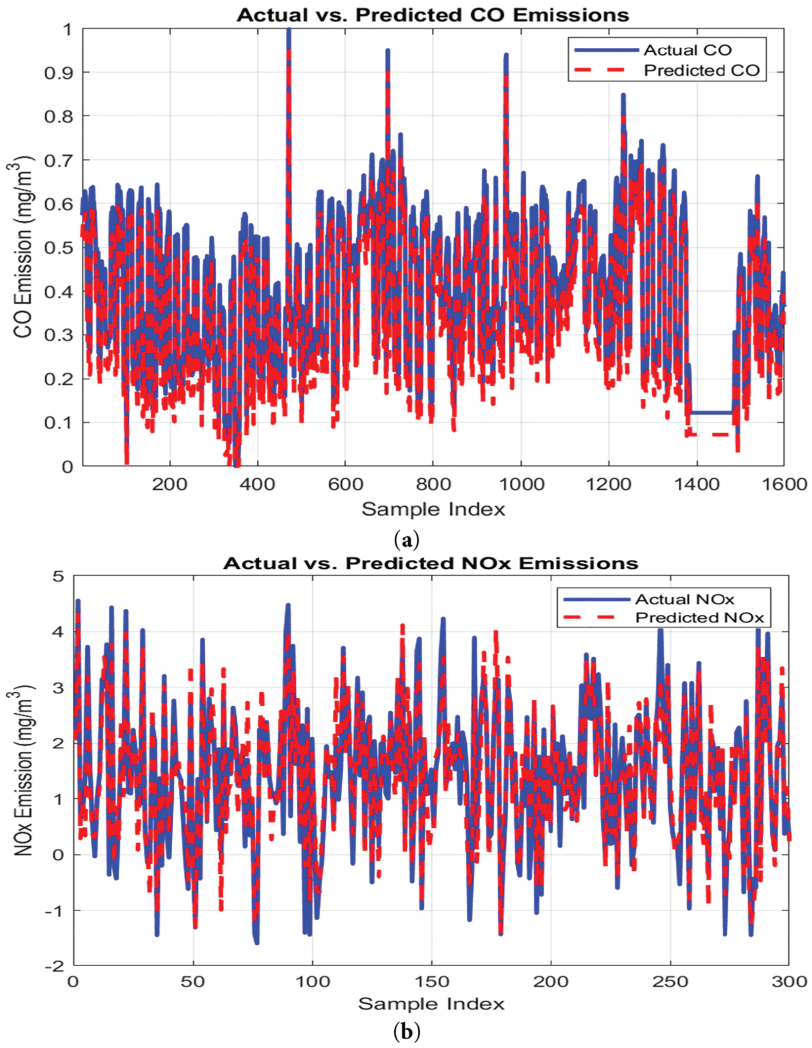


**Figure 2:** Actual vs. predicted (**a**) CO and (**b**) NOx emissions using IPSO-FFNN

### *7.2 Impact of PSO on FFNN Performance*

PSO played a pivotal role in enhancing the standard FFNN's prediction accuracy. By optimizing the network weights, PSO ensured faster convergence and minimized the risk of overfitting. Fig. 3 shows the loss (MSE) reduction during the training process, comparing IPSO-FFNN with standard FFNN.

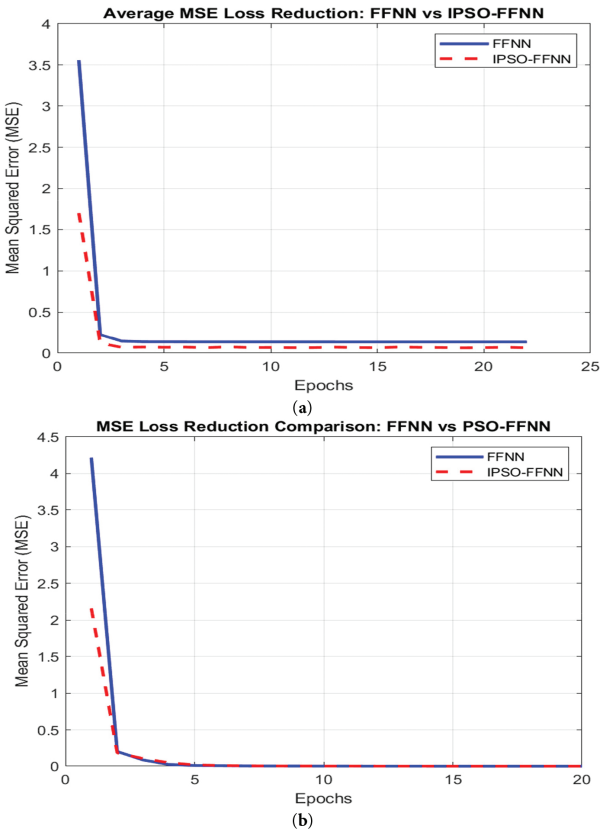


**Figure 3:** MSE loss reduction for (**a**) CO and (**b**) NOx: IPSO-FFNN vs. standard FFNN

The above figures demonstrate the trends in MSE loss reduction for IPSO-FFNN and standard FFNN models. The IPSO-FFNN shows a sharper decline in MSE during the initial epochs, indicating faster convergence due to the effective weight optimization achieved by the PSO algorithm. By the end of the training, the IPSO-FFNN achieves consistently lower MSE values, reflecting its superior accuracy and robustness in modeling emission dynamics. This improvement can be attributed to PSO's global search capability, which optimally adjusts the network weights, avoids suboptimal solutions, and mitigates the risk of getting trapped in local minima (challenges commonly faced by standard backpropagation). Additionally, the IPSO-FFNN stabilizes at a lower final loss, underscoring its enhanced generalization capability.

### *7.3 Error Analysis*

Error analysis reveals how well the IPSO-FFNN performs across different parts of the data, including handling outlier values. Table 9 shows the percentage reduction in errors (MSE, MAE, RMSE, MAPE, and $R^2$) when using the IPSO-FFNN compared to a standard FFNN for both CO and NOx predictions.

**Table 9:** Percentage reduction in error metrics by IPSO-FFNN compared to standard FFNN

| Emission type | Reduction in MSE (%) | Reduction in MAE (%) | Reduction in RMSE (%) | Reduction in MAPE (%) | Reduction in $R^2$ (%) |
|---|---|---|---|---|---|
| CO | 97.80 | 95.00 | 85.19 | 71.49 | 97.58 |
| NOx | 97.16 | 93.47 | 83.15 | 75.86 | 97.04 |

These reductions underline the IPSO-FFNN's effectiveness in minimizing prediction errors. The error analysis further indicated that IPSO-FFNN outperforms other models due to its ability to explore a diverse search space and escape local minima, resulting in improved generalization. The concentration of errors around zero, seen in Fig. 4, underscores the model's reliability.

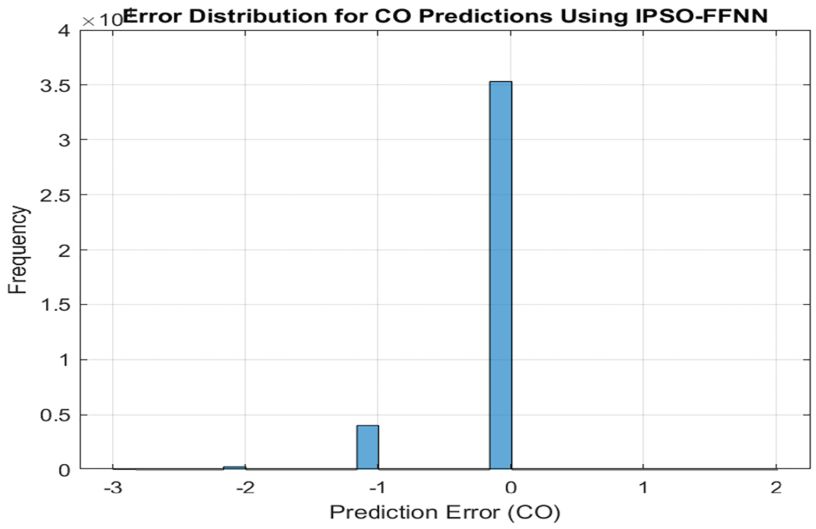


(**a**)

(**b**)

**Figure 4:** Error distribution for (**a**) CO and (**b**) NOx predictions using IPSO-FFNN

The error distribution shows that most errors are concentrated around zero, indicating minimal deviation from actual values, with only a few slight underestimations observed for both CO and NOx. This narrow error distribution highlights the model's reliability in predictions.

### *7.4 Comparative Evaluation of the Developed Model*

To comprehensively validate the performance of the IPSO-FFNN model, a comparative analysis was conducted against other models, including the Standard FFNN, Support Vector Regression (SVR), K-Nearest Neighbors (K-NN), and Long Short-Term Memory (LSTM) networks, using the same Exhaust Emission Dataset [37]. This evaluation was based on RMSE for predicting CO and NOx emissions, as detailed in Table 10. Additionally, a bar chart was generated in Fig. 5 to visually represent the RMSE performance across different models, highlighting the IPSO-FFNN model's superior accuracy.

**Table 10:** Comparative performance of IPSO-FFNN vs. other models (RMSE)

| Model | CO prediction (RMSE) | NOx prediction (RMSE) |
|---|---|---|
| Standard FFNN | 2.399 | 2.186 |
| IPSO-FFNN | 0.355 | 0.368 |
| SVR | 0.875 | 4.202 |
| K-NN | 1.499 | 1.521 |
| LSTM | 0.537 | 0.757 |

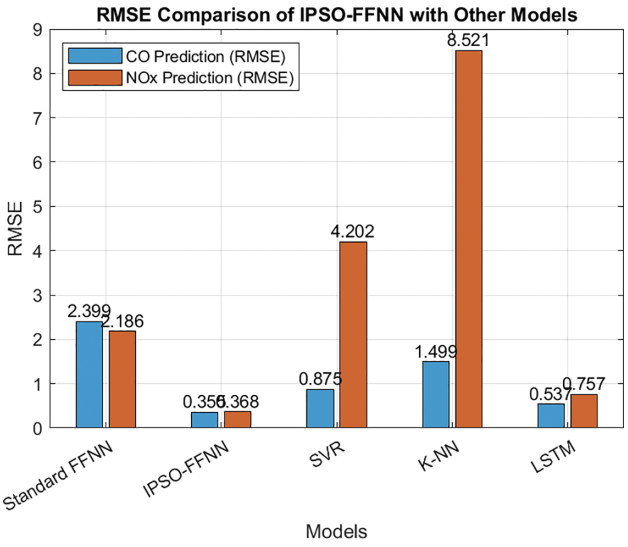


**Figure 5:** RMSE comparison of IPSO-FFNN with other models

The bar chart demonstrates that IPSO-FFNN produces the lowest RMSE values for both CO and NOx predictions, which proves its superior accuracy compared to other models.

The hybrid structure of IPSO-FFNN produces better results than other models. The PSO component performs global weight optimization to stop the model from getting stuck in local minimum points, which

standard FFNN and SVR models experience during highly nonlinear operations. The K-NN guided initialization method uses statistical methods to establish weight values, which leads to better model convergence and produces more stable predictions when turbine loads and environmental conditions change.

The IPSO-FFNN model generates more accurate NOx predictions than LSTM because the emission data points were recorded at one-hour intervals, which reduces the ability of LSTM to detect long-term patterns. After all, it weakens its capacity to identify complex nonlinear relationships between operational variables. The IPSO-FFNN model directly analyzes nonlinear relationships to generate better emission predictions.

## 8 Conclusions

This study successfully developed and implemented an intelligent monitoring system for predicting CO and NOx emissions in natural gas power plants using a hybrid model of improved PSO combined with FFNN. The use of real operational data demonstrated the model's practicality in real-world conditions, highlighting significant improvements in prediction accuracy. Key improvements included reduced prediction errors, enhanced model stability, and faster convergence. This approach introduces distinct contributions by integrating PSO's global optimization capability with FFNN's nonlinear learning potential, effectively addressing challenges such as local minima and suboptimal convergence. The study achieves its main methodological strength through the complete combination of NCA feature selection with PSO global optimization and FFNN nonlinear learning and K-NN residual error correction into a unified predictive system. The model achieves three key benefits through this integration because it learns complex emission patterns while optimizing its learning process and reducing prediction mistakes when operating conditions change.

The IPSO-FFNN model's real-time applicability allows continuous monitoring and early detection of abnormal emissions, enhancing environmental safety by minimizing pollutant leaks and ensuring compliance with stringent environmental standards. Beyond the energy sector, industries such as chemical processing, petrochemical refining, and waste management could adopt this model for emission control and operational efficiency, where real-time monitoring is critical.

However, certain limitations remain, including reliance on publicly available datasets and the constraints of the FFNN architecture. Future research should focus on model expansion to predict sulfur oxides (SOx) and particulate matter alongside its current pollutant prediction capabilities. Furthermore, future research should focus on direct hardware integration with turbine controllers and field-programmable gate arrays (FPGAs) to reduce response time and boost real-time performance. Additionally, advanced optimization methods such as Differential Evolution and Bayesian Optimization should be investigated to enhance both the speed and stability of convergence. The financial benefits of deploying the proposed intelligent monitoring system can be evaluated through economic frameworks that include the 'Option Value' concept when dealing with unpredictable environmental and market scenarios [49].

Moving forward, it is recommended that the IPSO-FFNN model be integrated into the monitoring systems of gas-fired power plants for real-time emission tracking and predictive maintenance. This integration would allow operators to make timely adjustments, minimize environmental impact, and optimize turbine operations. The conclusion establishes practical deployment as its focus while directing future research to expand models and study their economic viability.

**Acknowledgement:** The authors utilized AI-based language editing tools to enhance the manuscript's readability and presentation. No scientific content or data interpretation was generated by the AI.

**Funding Statement:** The authors received no specific funding for this study.

**Author Contributions:** The authors confirm contribution to the paper as follows: Conceptualization, Samar Taha Yousif and Firas Basim Ismail; methodology, Samar Taha Yousif; software, Samar Taha Yousif; validation, Samar Taha Yousif, Ammar Al-Bazi, and Alaa Abdulhady Jaber; formal analysis, Samar Taha Yousif; investigation, Samar Taha Yousif and Sivadass Thiruchelvam; resources, Firas Basim Ismail; data curation, Ammar Al-Bazi; writing—original draft preparation, Samar Taha Yousif; writing—review and editing, Firas Basim Ismail and Alaa Abdulhady Jaber; visualization, Ammar Al-Bazi; supervision, Firas Basim Ismail; project administration, Firas Basim Ismail. All authors reviewed the results and approved the final version of the manuscript.

**Availability of Data and Materials:** Not applicable.

**Ethics Approval:** Not applicable.

**Conflicts of Interest:** The authors declare no conflicts of interest to report regarding the present study.

## References

1. Bouza E, Vargas F, Alcázar B, Álvarez T, Asensio Á, Cruceta G, et al. Air pollution and health prevention: a document of reflection. Rev Esp Quimioter. 2022;35(4):307–32. doi:10.37201/req/171.2021.
2. Larki I, Zahedi A, Asadi M, Forootan MM, Farajollahi M, Ahmadi R, et al. Mitigation approaches and techniques for combustion power plants flue gas emissions: a comprehensive review. Sci Total Environ. 2023;903:166108. doi:10.1016/j.scitotenv.2023.166108.
3. Salman NA, Al-mishrey MK, Al-saad HT. Air pollution in the southern part of Iraq and its health risks. In: Aerosol optical depth and precipitation. Berlin/Heidelberg, Germany: Springer; 2024. p. 107–22. doi:10.1007/978-3-031-55836-8.
4. Babaee S, Loughlin DH. Exploring the role of natural gas power plants with carbon capture and storage as a bridge to a low-carbon future. Clean Technol Environ Policy. 2017;19(2):629–42. doi:10.1007/s10098-017-1479-x.
5. Nemitallah MA, Rashwan SS, Ibrahim B, Abdelhafez AA, Habib MAM. Review of novel combustion techniques for clean power production in gas turbines. Energy Fuels. 2018;32(2):979–1004. doi:10.1021/acs.energyfuels.7b03607.
6. Zeinalipour K, Barriere L, Ghelardi D, Gori M. Application of machine learning models for carbon monoxide and nitrogen oxides emission prediction in gas turbines. arXiv:2501.17865. 2025.
7. Tuttle JF. Sustainable NOx emission reduction at a coal-fired power station through the use of online neural network modeling and particle swarm optimization. Control Eng Pract. 2019;93(4):104177. doi:10.1016/j.conengprac.2019.104177.
8. Solanke B, Onita FB, Ochulor OJ, Iriogbe HO, Shell T. The impact of artificial intelligence on regulatory compliance in the oil and gas industry. Int J Sci Technol Res Arch. 2024;7(1):61–72. doi:10.53771/ijlsra.2024.7.1.0059.
9. Park S, Choi GM, Tanahashi M. Demonstration of a gas turbine combustion-tuning method and sensitivity analysis of the combustion-tuning parameters with regard to NOx emissions. Fuel. 2019;239(62):1134–42. doi:10.1016/j.fuel.2018.11.021.
10. Potts R, Hackney R, Leontidis G. Tabular machine learning methods for predicting gas turbine emissions. Mach Learn Knowl Extrac. 2023;5(3):1055–75. doi:10.3390/make5030055.
11. Vault T, Theses O. Data-driven approach for emission monitoring and management [dissertation]. Calgary, AB, Canada: University of Calgary; 2023.
12. Lim S. Hybrid neural network-based maritime carbon dioxide emission prediction: incorporating dynamics for enhanced accuracy. Appl Sci. 2022;15(9):4654. doi:10.3390/app15094654.
13. Rezazadeh A. Environmental pollution prediction of NOx by predictive modelling and process analysis in natural gas turbine power plants. Pollution. 2021;7(2):481–94. doi:10.22059/poll.2021.316327.977.
14. Barboza ABV, Mohan S, Dinesha P. On reducing the emissions of CO, HC, and NOx from gasoline blended with hydrogen peroxide and ethanol: optimization study aided with ANN-PSO. Environ Pollut. 2022;310:119866. doi:10.1016/j.envpol.2022.119866.

15. Qiu S, Chen B, Wang R, Zhu Z, Wang Y, Qiu X. Atmospheric dispersion prediction and source estimation of hazardous gas using artificial neural network, particle swarm optimization and expectation maximization. Atmos Environ. 2018;178:158–63. doi:10.1016/j.atmosenv.2018.01.056.
16. Chen Q, Wang W. Prediction of shale gas horizontal well production using particle swarm optimisation-based BP neural network. Int J Oil Gas Coal Technol. 2024;36(4):449–60. doi:10.1504/IJOGCT.2024.142105.
17. Li Z, Fong RS, Fujiwara K, Aihara K, Tanaka G. Structuring multiple simple cycle reservoirs with particle swarm optimization. arXiv:2504.05347. 2025.
18. Kumar G, Singh UP, Jain S. Swarm intelligence-based hybrid neural network approach for stock price forecasting. Comput Econ. 2021;60(3):747–74. doi:10.1007/s10614-021-10176-9.
19. Jamous R, Alrahhal H, El-Darieby M. A new ANN-particle swarm optimization with center of gravity (ANN-PSOCoG) prediction model for the stock market under the effect of COVID-19. Sci Program. 2021;2021(53):6656150. doi:10.1155/2021/6656150.
20. Bardhan A, Samui P, Ghosh K, Gandomi AH, Bhattacharyya S. ELM-based adaptive neuro swarm intelligence techniques for predicting the California bearing ratio of soils in soaked conditions. Appl Soft Comput. 2021;110:107595. doi:10.1016/j.asoc.2021.107595.
21. Wang Y, Liu H, Yu ZX, Tu LP. An improved artificial neural network based on human-behaviour particle swarm optimization and cellular automata. Expert Syst Appl. 2020;140(1):112862. doi:10.1016/j.eswa.2019.112862.
22. Kayarvizhy N, Kanmani S, Uthariaraj RV. ANN models optimized using swarm intelligence algorithms. WSEAS Trans Comput. 2020;13:501–19.
23. Ghanem WAHM, Jantan A. A cognitively inspired hybridization of artificial bee colony and dragonfly algorithms for training multi-layer perceptrons. Cogn Comput. 2018;10(6):1287–1301. doi:10.1007/s12559-018-9588-3.
24. Moayedi H, Abdullahi MM, Nguyen H, Rashid ASA. Comparison of dragonfly algorithm and Harris hawks optimization evolutionary data mining techniques for the assessment of bearing capacity of footings over two-layer foundation soils. Eng Comput. 2023;37(1):437–47. doi:10.1007/s00366-019-00834-w.
25. Kareem SW. Novel swarm intelligence algorithms for structure learning of Bayesian networks and a comparative evaluation [dissertation]. Izmir, Türkiye: Yasar University; 2020.
26. Amadi FAJ, Ottaghi ZASAM, Ahmoodabadi MOJAM, Ohari TAZ, Agheri AHB. Long-term prediction of the crude oil price using a new particle swarm optimization algorithm. J Energy Manag Technol. 2020;5(1):17–23. doi:10.22109/jemt.2020.210651.1211.
27. Shah MI, Javed MF, Alqahtani A, Aldrees A. Environmental assessment-based surface water quality prediction using hyper-parameter optimized machine learning models based on consistent big data. Process Saf Environ Prot. 2021;151(4):324–40. doi:10.1016/j.psep.2021.05.026.
28. Ellahi M, Abbas G. A modified hybrid particle swarm optimization with bat algorithm parameter-inspired acceleration coefficients for solving eco-friendly and economic dispatch problems. IEEE Access. 2021;9:82169–87. doi:10.1109/access.2021.3085819.
29. Geetha U, Sankar S. Multi-objective modified particle swarm optimization for test suite reduction. Comput Syst Sci Eng. 2022;41(3):951–62. doi:10.32604/csse.2022.022621.
30. Tarkhaneh O, Shen H. Training of feedforward neural networks for data classification using hybrid particle swarm optimization, Mantegna Lévy flight and neighborhood search. Heliyon. 2019;5(4):e01275. doi:10.1016/j.heliyon.2019.e01275.
31. Norwahidayah S, Noraniah, Farahah N, Amirah A, Liyana N, Suhana N. Performances of artificial neural network (ANN) and particle swarm optimization (PSO) using KDD Cup '99 dataset in intrusion detection system (IDS). J Phys Conf Ser. 2023;1874(1):12061. doi:10.1088/1742-6596/1874/1/012061.
32. Kumar K, Singh V, Roshni T. Application of the PSO-neural network in rainfall–runoff modeling. Water Pract Technol. 2023;18(1):16–26. doi:10.2166/wpt.2022.155.
33. Guo F, Wang P, Tansey K, Zhang Y, Li M, Liu J, et al. A novel transformer-based neural network under model interpretability for improving wheat yield estimation using remotely sensed multi-variables. Comput Electron Agric. 2024;223(9):109111. doi:10.1016/j.compag.2024.109111.

34. Gkonis V, Tsakalos I. A hybrid optimized deep learning model via the golden jackal optimizer for accurate stock price forecasting. Expert Syst Appl. 2025;278(1):127287. doi:10.1016/j.eswa.2025.127287.
35. Hosseini E, Saeedpour B, Banaei M, Ebrahimy R. Optimized deep neural network architectures for energy consumption and PV production forecasting. Energy Strategy Rev. 2025;59(2):101704. doi:10.1016/j.esr.2025.101704.
36. Yousif ST, Alnaimi F, Bazi AAI, Thiruchelvam S. Enhancing power plants safety by accurately predicting CO and NOx leakages from gas turbines using FFNN and LSTM neural networks. Proc Int Workshop Simul Energy Sustain Dev Environ. 2023:1–9. doi:10.46354/i3m.2023.sesde.009.
37. Kaya H, Tüfekci P, Uzun E. Predicting CO and NOx emissions from gas turbines: novel data and a benchmark PEMS. Turk J Electr Eng Comput Sci. 2019;27(7):4783–96. doi:10.3906/elk-1807-87.
38. Adams D, Oh DH, Kim DW, Lee CH, Oh M. Prediction of SOx–NOx emission from a coal-fired CFB power plant with machine learning: plant data learned by deep neural network and least square support vector machine. J Clean Prod. 2020;270:122310. doi:10.1016/j.jclepro.2020.122310.
39. Bakay MS, Ağbulut Ü. Electricity production-based forecasting of greenhouse gas emissions in Turkey with deep learning, support vector machine and artificial neural network algorithms. J Clean Prod. 2020;125324. doi:10.1016/j.jclepro.2020.125324.
40. Yuan Z, Meng L, Gu X, Bai Y, Cui H, Jiang C. Prediction of NOx emissions for coal-fired power plants with stacked-generalization ensemble method. Fuel. 2020;282:119748. doi:10.1016/j.fuel.2020.119748.
41. Freida O, Victor B, Indati S, Fernando Y. Effect of activation function in modeling the nexus between carbon tax, $CO_2$ emissions, and gas-fired power plant parameters. Energy Convers Manage X. 2021;12(12):100111. doi:10.1016/j.ecmx.2021.100111.
42. Dirik M. Prediction of NOx emissions from gas turbines of a combined cycle power plant using an ANFIS model optimized by GA. Fuel. 2022;321(12):124037. doi:10.1016/j.fuel.2022.124037.
43. Ahmadi MH, Jashnani H, Chau KW, Kumar R, Rosen MA. Carbon dioxide emissions prediction of five Middle Eastern countries using artificial neural networks. Energy Sources Part A Recover Util Environ Eff. 2019;45(3):9513–25. doi:10.1080/15567036.2019.1679914.
44. Wood DA. Long-term atmospheric pollutant emissions from a combined cycle gas turbine: trend monitoring and prediction applying machine learning. Fuel. 2023;343(1):127722. doi:10.1016/j.fuel.2023.127722.
45. Moliere M, Jaubert JN, Privat R, Schuhler T. Stationary gas turbines: an exergetic approach to part load operation. Oil Gas Sci Technol. 2020;75(3):1–11. doi:10.2516/ogst/2020001.
46. Shami TM, El-saleh AA. Particle swarm optimization: a comprehensive survey. IEEE Access. 2022;10:10031–61. doi:10.1109/ACCESS.2022.3144567.
47. Nino-Adan I, Portillo E, Landa-Torres I, Manjarres D. Normalization influence on ANN-based models performance: a new proposal for features' contribution analysis. IEEE Access. 2021;9:125462–77. doi:10.1109/ACCESS.2021.3110647.
48. Awasthi P, Das A, Sen R, Suresh AT. On the benefits of maximum likelihood estimation for regression and forecasting. arXiv:2106.10370. 2021. doi:10.48550/arXiv.2106.10370.
49. Borozan S, Giannelos S, Aunedi M, Strbac G. Option value of EV smart charging concepts in transmission expansion planning under uncertainty. In: 2022 IEEE 21st Mediterranean Electrotechnical Conference (MELECON); 2022 Jun 14–16; Palermo, Italy. p. 63–8. doi:10.1109/MELECON53508.2022.9842982.